Analytical Methods

Cite this: *Anal. Methods*, 2012, **4**, 3653

www.rsc.org/methods

PAPER

Graphene impregnated with horseradish peroxidase multimer for the determination of hydrogen peroxide†‡

Yogeswaran Umasankar,§ Binesh Unnikrishnan, Shen-Ming Chen* and Tzu-Wei Ting

Received 18th March 2012, Accepted 23rd August 2012
DOI: 10.1039/c2ay25276g

Horseradish peroxidase (HRP) multimer on a graphene modified glassy carbon electrode (GCE) has been fabricated by carbodiimide coupling reaction. The possible adsorption sites of HRP on graphene were predicted by Lamarckian genetic algorithm. It has been observed that HRP has five possible sites for its adsorption to graphene. Scanning electron microscopy and atomic force microscopy measurements support the evidence of formation of HRP multimer graphene. The graphene–HRP multimer film showed good electrocatalytic activity for the reduction of hydrogen peroxide. The electrochemical studies showed that graphene on the GCE increased the effective surface area, reduced the charge transfer resistance of the electrode and enhanced the electrochemical signal. The detection limit of H_2O_2 (9 nM) at graphene–HRP multimer was also lower than that of other electrodes studied in this work. The sensitivity of the graphene–HRP multimer film towards H_2O_2 determination was 7.8 μA μM^{-1} cm^{-2}. Differential pulse voltammetry and selectivity studies revealed that GCE modified by graphene–HRP multimer film can be efficiently used for H_2O_2 determination in real samples.

1. Introduction

Graphene is a two dimensional sheet of carbon atoms with sp^2 bonds arranged in a hexagonal structure. Graphene has extraordinary properties, such as large surface area, high mechanical strength and high elasticity.[1,2] Among various graphene structures, the electrochemistry of multilayer graphene is as important as that of graphene. Similarly to carbon nanotubes (CNT), graphene sheets have edge planes which have excellent electrochemical properties; however, the basal plane of graphene has no such electrochemical properties.[2] Graphene's heterogeneous electron transfer is also faster than that of CNT, because of the greater number of edges in the graphene structure.[3,4] The above mentioned electrochemical properties of graphene matrices have received considerable attention in recent years. Various electrodes modified with graphene have been synthesized for the electrochemical determination of chemical and biochemical compounds, where the graphene matrix acts as an electrocatalyst.[5–8]

Horseradish peroxidase (HRP) is a member of the peroxidases which is also an oxidoreductase enzyme and an electron acceptor compound. HRP forms an enzymatic oxidizing agent containing oxyferryl heme and porphyrin radical in the presence of H_2O_2. This enzymatic oxidizing agent is catalytically active and takes an electron from the substrate and forms a second intermediate, which reduces back to the native enzyme (Fe^{III}) by receiving another electron from the substrate.[9] This redox reaction of HRP has been widely utilized in biosensors for H_2O_2 determination.[10] In biological systems, H_2O_2 is the most valuable marker for oxidative stress.[11,12] Generally, H_2O_2 is also present in underground and rainwater as a result of pollution from industries and atomic power stations. These factors increase the necessity for the quantitative measurements of H_2O_2.[13,14] As a result, electrocatalytic reduction and accurate determination of H_2O_2 at low potential constitute a valuable task and there is an ongoing search for sensitive and selective methods. Other major applications of electrocatalysis of O_2 and H_2O_2 reduction are in fuel cells.

A carbodiimide coupling reaction involving *N*-ethyl-*N*′-(3-dimethylaminopropyl) carbodiimide (EDC) and *N*-hydroxysuccinimide (NHS) is one of the methods employed for coupling carboxylic acid groups containing matrices with enzymes.[15–17] In this coupling reaction, the EDC/NHS cross-linking agents introduce amide cross-links between carboxylic acid groups and amino acid residues present in the enzyme.[18] The carbodiimide coupled enzyme hybrid matrices have good electrocatalytic properties.[17] Furthermore, EDC/NHS cross-linked collagens are

Electroanalysis and Bioelectrochemistry Lab, Department of Chemical Engineering and Biotechnology, National Taipei University of Technology, No. 1, Section 3, Chung-Hsiao East Road, Taipei-106, Taiwan (ROC). E-mail: smchen78@ms15.hinet.net; Fax: +886 2270 25238; Tel: +886 2270 17147

† This article is part of a web theme in *Analyst* and *Analytical Methods* on Future Electroanalytical Developments, highlighting important developments and novel applications. Also in this theme is work presented at the Eirelec 2011 meeting, dedicated to Professor Malcolm Smyth on the occasion of his 60th birthday.

‡ Electronic supplementary information (ESI) available. See DOI: 10.1039/c2ay25276g

§ Present address: College of Engineering, University of Georgia, Athens, GA 30602, United States.

reported to be non toxic and biocompatible.[19–21] In the present work, instead of coupling an enzyme with a matrix, two or more HRP have been coupled to form an enzyme multimer. The prepared HRP multimer was immobilized on graphene matrix by van der Waals interactions. A thorough survey of the literature reveals that there have been no previous attempts made to prepare HRP multimer or graphene–HRP multimer films. The graphene matrix was chosen as an immobilization matrix because of its excellent electrochemical properties. In this paper, we report the fabrication, characterization, electrochemical and electrocatalytic properties of graphene–HRP multimer film. The application of graphene–HRP multimer for real sample analysis has also been reported.

2. Experimental

2.1. Materials

Graphene dispersion (PureSheets MONO, average flake area = ~10 000 nm^2) obtained from NanoIntegris was used as received. HRP, EDC, NHS and H_2O_2 obtained from Aldrich and Sigma-Aldrich were also used as received. All other chemicals used were of analytical grade. The aqueous solutions were prepared with twice distilled deionized water. Solutions were deoxygenated by purging with pre-purified nitrogen gas. Phosphate buffer solution (PBS) pH 7.0 was prepared from 0.1 M Na_2HPO_4 and 0.1 M NaH_2PO_4 aqueous solutions.

2.2. Apparatus

Cyclic voltammetry (CV) and differential pulse voltammetry (DPV) were performed using analytical system models CHI-1205 and CHI-750 potentiostats respectively. A conventional three-electrode cell assembly consisting of an Ag/AgCl reference electrode and a Pt wire auxiliary electrode was used for electrochemical measurements. The working electrode was glassy carbon electrode (GCE) modified either with graphene, graphene–HRP (composite-1), graphene–EDC–NHS (composite-2) or graphene–HRP multimer (composite-3) films. For all the experimental results, potential is reported with respect to Ag/AgCl reference electrode. Electrochemical impedance spectroscopy (EIS) measurements were performed using IM6ex ZAHNER (Kroanch, Germany). The morphological characterizations of various films were done by means of scanning electron microscopy (SEM) (Hitachi S-3000H) and atomic force microscopy (AFM) (Being Nano-Instruments CSPM4000). Raman spectrum was acquired using Micro-Raman spectrometer (RENISHAW in Via system, U.K) by a 514.4 nm He/Ne laser. All the measurements were carried out at 25 °C ± 2.

2.3. Preparation of graphene–HRP multimer film modified electrode

Preparation of graphene–HRP multimer film modified GCE was carried out by systematic consecutive steps. The GCE was polished well using a Bioanalytical Systems (BAS) polishing kit with 0.05 μm alumina slurry, and then rinsed and ultrasonicated in deionized water. Then, 1.25 μg cm^{-2} of graphene was uniformly coated on the GCE using homogeneous graphene dispersion and dried at room temperature. The homogeneous graphene dispersion, in which the graphene was dispersed in ionic type surfactant solution, was obtained from NanoIntegris. 2 μl of 0.4 M EDC and 0.1 M NHS solution mixture was drop cast onto graphene modified GCE. Following the EDC/NHS addition, 25 μg cm^{-2} of HRP was dropped from HRP solution. Then the EDC/NHS/HRP solution mixture on the graphene modified GCE surface was allowed to react at room temperature for 4 h to form HRP multimer on the graphene (composite-3). The modified composite-3 GCE was then carefully washed with deionized water to remove EDC and NHS. Composite-1 film modified GCE was prepared by coating 25 μg cm^{-2} of HRP over graphene modified GCE. Similarly, composite-2 film was prepared by coating 2 μl of 0.4 M EDC and 0.1 M NHS solution mixture on graphene modified GCE and dried at 25 °C. The composite-2 film has been studied to understand the electrochemical and morphological changes occurring in graphene matrix due to the presence of EDC and NHS during the composite-3 film preparation.

3. Results and discussions

3.1. Preparation and characterization of HRP multimer on graphene modified electrode

The preparation of HRP multimer on graphene modified GCE was carried out by a carbodiimide coupling reaction using EDC, in which NHS was added to assist the carbodiimide coupling.[15] Briefly, in a carbodiimide coupling reaction, the EDC converts the carboxylic acid group into a reactive intermediate which is susceptible to reaction with primary amines. EDC cross linking is most efficient in acidic conditions, particularly at pH 4.5, and 4-morpholinoethanesulfonic acid buffer is suitable. PBS with neutral pH is also compatible with the EDC reaction; however, the efficiency is lower. An increased amount of EDC in the reaction mixture can compensate for the reduced efficiency, therefore a higher concentration of EDC has been used in this experiment. At physiological pH the reactive intermediate formed in the presence of NHS is more stable than in its absence. Thus, NHS increases the efficiency and yield of the coupling reaction.[22]

Among the twenty different amino acids in HRP, aspartic acid and glutamic acid have free carboxylate groups without any peptide linkage. Both these amino acids are considered to be carboxylate group donors for the coupling reaction. Similarly, lysine present in the HRP has free primary amine groups without any peptide linkage, and it is involved in the coupling reaction.[18] The other amino acids present in the HRP such as alanine, cysteine, glycine, *etc.*, do not have any free carboxylate groups or primary amine groups without peptide linkage, so they are not involved in the carbodiimide coupling reaction. Since neutral pH conditions are used, the possibility of hydrolysis of amide groups and their participation in the coupling reaction can be eliminated. The three step carbodiimide coupling mechanism for HRP multimer formation is given in Fig. 1. Step 1: the free carboxylate groups present on the outer surface of HRP react with EDC to form active intermediates. Step 2: these active intermediates undergo a condensation reaction with NHS and form amine reactive sulfo-NHS ester. Step 3: these amine reactive ester intermediates react with free amine groups present on the neighbouring HRPs to form the HRP multimer coupled through amide bonds.

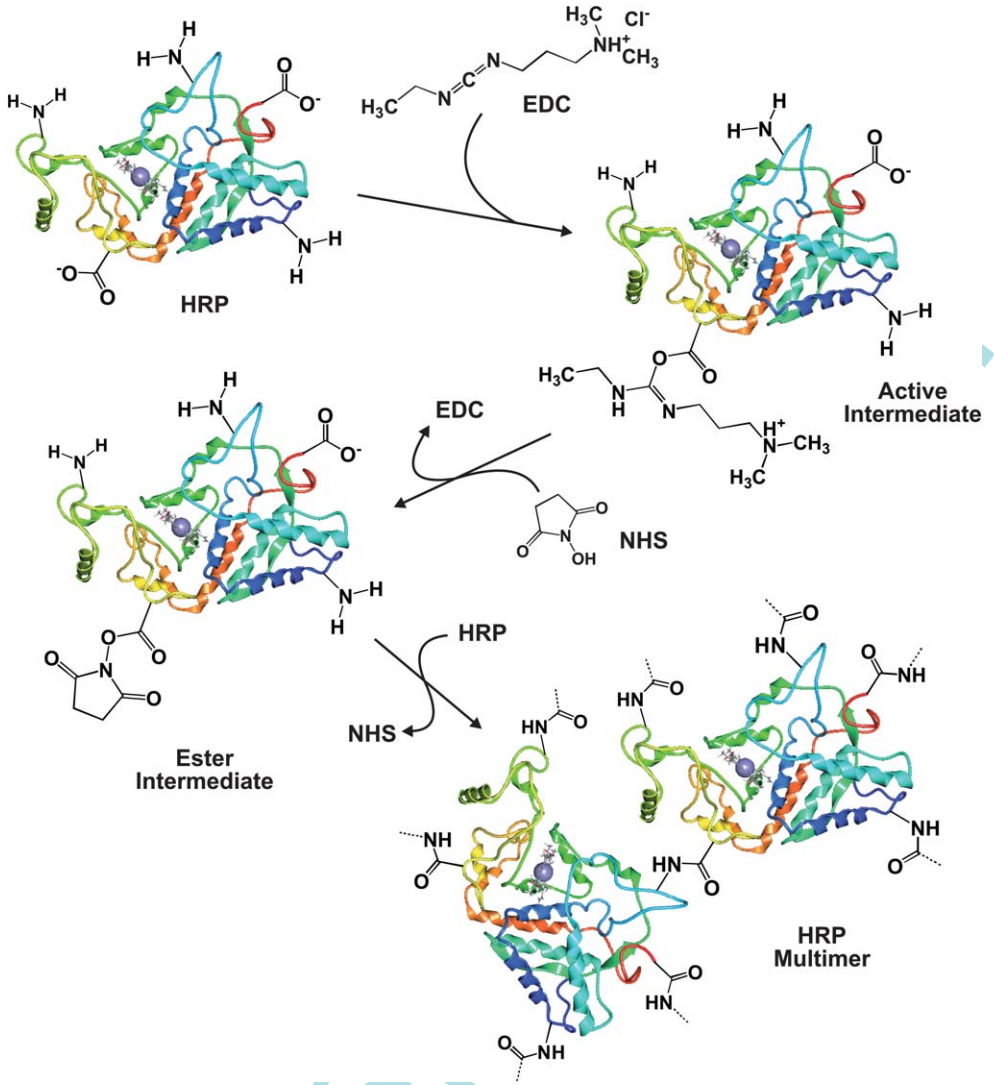

Fig. 1 Carbodiimide coupling reaction mechanism for HRP multimer formation.

These HRP multimer formation reactions, described above, were carried out on the graphene modified GCE surface. Computer simulation experiments were carried out to understand the structural interaction between graphene and HRP. The possible adsorption sites of graphene (G1 to G5) on HRP monomer are given in Fig. 2(a). In these simulation experiments, HRP monomer was used instead of HRP multimer to reduce complications and to understand the binding sites on a single HRP. The simulation was carried out using Lamarckian genetic algorithm,[23,24] where many double layer graphene molecules were docked on HRP. The simulation conditions such as population size (50), maximum generations (3000), crossover rate (0.8), mutation rate (0.2), elitism (5), local search rate (0.06) and local search maximum steps (100) were kept constant and the area around the binding site was maintained in the ratio of 9 × 9 × 9 nm for all the experiments. The results reveal that among numerous graphene sheets used in docking experiments (not shown in figure), five graphene sheets adsorb on the HRP with minimum free energies of −23.54 (G1), −16.43 (G2), −15.74 (G3), −17.36 (G4) and −16.71 kcal mol^{-1} (G5). These five sheets represent the five possible adsorption sites on HRP for double layer graphene sheets. In these simulation experiments double layer graphene sheets were used as a model because a high ratio of double layer graphene was present in the dispersion.

Graphene, composite-1, 2 and 3 film modified and bare GCEs were characterized by CV. The cyclic voltammograms presented in the inset of Fig. 3 are the redox reactions of $Fe^{III/II}$ at composite-1 and 3 modified GCEs (composite-2, graphene and bare GCE are given in ESI‡). From the current values obtained from cyclic voltammograms and by using Randles–Sevcik equation, the effective area of the above mentioned modified and unmodified GCEs are calculated. The effective area of bare GCE, graphene, composite-1, 2 and 3 are 0.19, 0.20, 0.14, 0.21 and 0.22 mm^2 respectively. These results show that the presence of HRP multimer on the electrode gives higher effective area than that of the HRP monomer on the electrode, which in turn would enhance the electrocatalysis of analyte. Similarly, the presence of graphene also enhances the effective area.

The EIS was carried out to study the charge transfer resistance of bare GCE, graphene, composite-1, 2 and 3 modified GCEs.

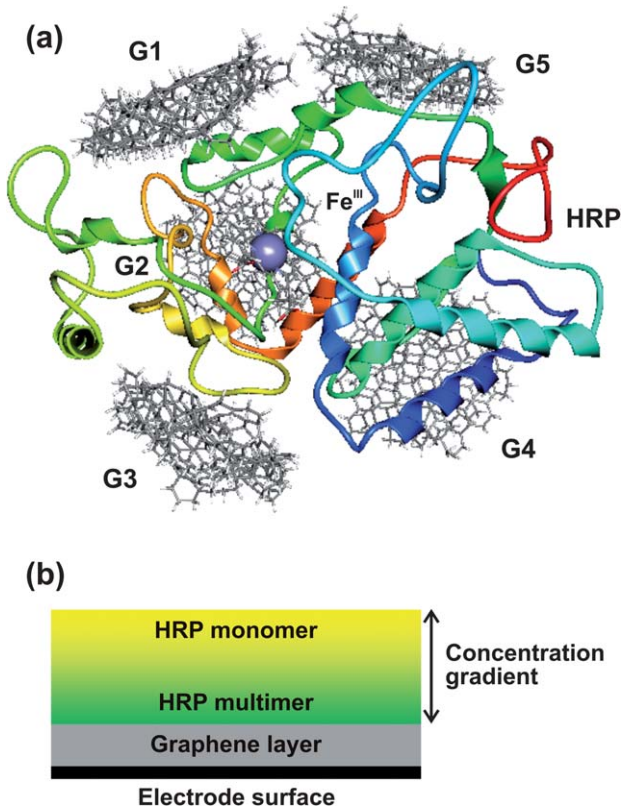

Fig. 2 (a) Possible adsorption sites of graphene (G1–G5) at HRP given by Lamarckian genetic algorithm, (b) composition and concentration gradient of composite-3 film modified electrode.

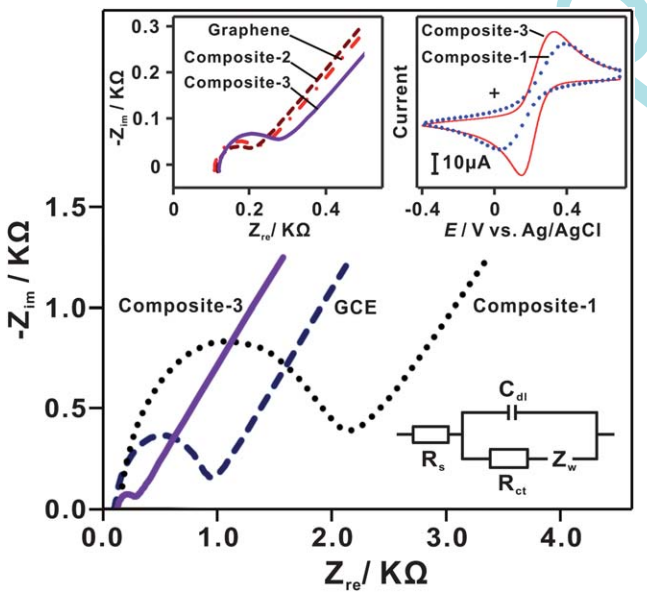

Fig. 3 Nyquist plots of bare GCE, composite-1 and composite-3 modified GCEs in 5 mM $[Fe(CN)_6]^{3-/4-}$ in PBS. Amplitude: 5 mV, frequency: 0.1 Hz to 1 MHz. Top left inset shows the Nyquist plots of graphene, composite-2 and 3 modified GCE. Top right inset is the cyclic voltammograms of composite-1 and 3 modified GCEs at 50 mV s^{-1} in the same electrolyte. The bottom right inset is Randles equivalence circuit for the above mentioned electrodes.

Fig. 3 and its top left inset shows the impedance spectra represented as Nyquist plots (Z_{re} *vs.* Z_{im}) for the above mentioned modified and unmodified GCEs in 5 mM $[Fe(CN)_6]^{3-/4-}$. The bottom right inset in Fig. 3 represents the Randles equivalent circuit model used to fit the experimental data, where R_s is electrolyte resistance, R_{ct} charge transfer resistance, C_{dl} double layer capacitance and Z_w Warburg impedance. The curves which appear in the Nyquist plots indicate the parallel combination of charge transfer resistance and double layer capacitance resulting from electrode impedance.[25] As shown in Fig. 3, all the electrodes exhibit curves of various sizes in the frequency range from 0.1 Hz to 1 MHz. The size of the curve (diameter of the semicircle portion) for composite-1 is higher than all other modified and unmodified GCEs, which reveals the charge transfer resistance due to HRP monomer on the electrode surface. This higher R_{ct} value is an indication of immobilized enzyme. Similarly, R_{ct} result for composite-3 can be seen in the top left inset of Fig. 3, which also indicates enzyme immobilization. However, when comparing the curve size of composite-1 and 3, composite-3 has lower area because of its reduced electron transfer resistance. The size of curves obtained was in the order of composite-1 > bare GCE > composite-3 > graphene > composite-2. In order to find the electron transfer efficiency of the electrodes, the R_{ct} values were obtained for both modified and unmodified electrodes by fitting the Nyquist plot results with Randles equivalent circuit model. The obtained R_{ct} values of bare GCE, graphene, composite-1, 2 and 3 with respect to their effective area are 39.2, 4.8, 125.2, 2.6 and 6.0 kΩ cm^{-2} respectively. The above values reveal that the R_{ct} in presence of HRP multimer (in composite-3) is lower than HRP monomer (in composite-1). Similarly the presence of graphene also reduces the R_{ct}. These results prove that the HRP multimer and graphene present on GCE enhances electron shuttling between reactant and the electrode surface. Thus, composite-3 film modified GCE has excellent electrochemical properties, such as high effective area and faster electron transfer rate. These electrochemical properties are useful for the electrocatalysis of analyte.

3.2. Morphology of graphene and its composite films

Graphene, composite-2 and 3 films were prepared on indium tin oxide (ITO) electrodes with the same experimental conditions as that of GCE, and the modified electrodes were characterized using SEM and AFM techniques. The top views of microstructures on the ITO electrode surface in Fig. 4(a)shows the presence of micro-size flakes of graphene deposited from a uniform dispersion. The presence of graphene was confirmed by the characteristic bands[26,27] obtained in Raman spectrum (see ESI‡). As mentioned in section 2.3, the composite-2 film was studied to understand the influence of EDC and NHS over graphene matrix structure. Fig. 4(b) reveals that coagulation of graphene flakes occurred after the addition of EDC and NHS over graphene matrix. However, this coagulation would not affect the catalytic property of graphene, because the EDC and NHS were washed away after the cross-linking of HPR. Finally, because a concentration gradient exists between HRP monomer and multimer during film preparation, the surface of composite-3 (Fig. 4(c)) looks similar to the surface of HRP.[28] This concentration gradient, displayed in Fig. 2(b), could occur due to low

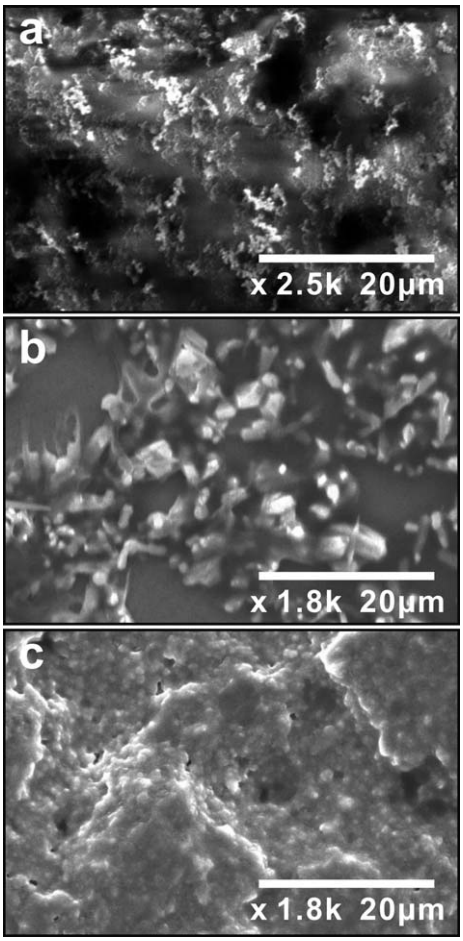

Fig. 4 SEM images of (a) graphene, (b) composite-2 and (c) composite-3 films.

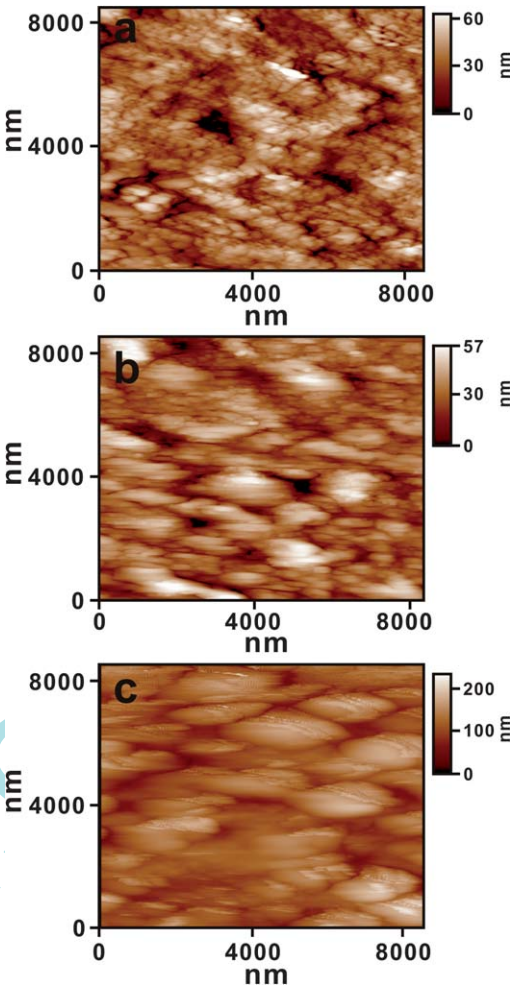

Fig. 5 AFM images of (a) graphene, (b) composite-2 and (c) composite-3 films.

access of EDC and NHS in the top layer of HRP solution during film preparation process. The magnified view of the images of the same three modified electrodes by AFM, shown in Fig. 5(a)–(c), also reveals the difference in surface structures.

The morphologies of all three modified electrodes obtained using AFM were similar to the results obtained using SEM. The thickness of graphene, composite-2 and composite-3 films obtained using AFM results were 60, 57 and 232 nm respectively. These values show that composite-3 film is thicker than the other two films. The thickness of the concentration gradient layer displayed in Fig. 2(b) was ~173 nm (±3). These SEM and AFM results reveal the coexistence of graphene and HRP in the composite film.

3.3. Electrochemical and pH studies of graphene–HRP multimer film

The cyclic voltammograms of composite-3 modified GCE in PBS at different scan rate show that the anodic and cathodic peak currents of the $Fe^{III/II}$ redox couple of the heme group in HRP increase linearly with increasing scan rate (figure not shown). The ratio of I_{pa}/I_{pc} for composite-3 film demonstrates that the redox process was not controlled by diffusion until 300 mV s^{-1}. However, the peak separation, ΔE_p, of the redox couple increases as the scan rate increases (see ESI‡). The effect of pH on composite-3 film was also studied, as the cyclic voltammograms of composite-3 modified GCE were obtained in various pH aqueous buffer solutions (see ESI‡). The composite-3 film preparation was carried out as described in section 2.3, and then washed with deionized water before transferring it into various pH solutions. The results show that the film is stable in a pH range between 5 and 9. The values of E_{pa} and E_{pc} depend on the pH of the buffer solution, and the I_{pc} of composite-3 was higher in pH 7.0 than in other pH solutions. The response from the plot of formal potential ($E^{\circ\prime}$) *vs.* pH shows a slope of 59.6 mV pH^{-1}, which is close to the theoretical value given by Nernstian equation for equal number of electrons and protons transfer.

3.4. Electroanalytical response of H_2O_2 at graphene and its composite films

The graphene, composite-1 and 3 film modified GCEs were prepared at similar conditions, as given in section 2.3. These film modified GCEs were then washed carefully in deionized water and transferred to PBS for the electrocatalytic studies of H_2O_2. All the cyclic voltammograms were recorded at a constant time interval of 1 min with N_2 purging before the start of each

experiment. Fig. 6 shows the electrocatalytic reduction of H_2O_2 (0.22 μM) at various film modified and bare GCEs with a scan rate of 50 mV s^{-1}. The film modified GCEs tested were graphene, composite-1 and 3 films. For composite-3 film, cyclic voltammograms are shown for both the presence and absence of H_2O_2. The cyclic voltammogram for composite-3 film exhibits reversible redox couples in the absence of H_2O_2. Upon addition of H_2O_2, a growth in the reduction peak of H_2O_2 appears at $E_{pc} = -260$ mV. However, there is no H_2O_2 reduction peak for bare GCE, graphene and composite-1 films. For composite-3 film, an increase in concentration (34 nM to 0.22 μM) of H_2O_2 simultaneously produced a linear increase in reduction peak current of H_2O_2 with good film stability. However, there is a decrease in the peak current for composite-1 film as shown in the inset of Fig. 6. These results prove that the electrocatalytic reduction of H_2O_2 takes place at composite-3 film modified GCE, but not at the other three electrodes.

From the slopes of the linear calibration curve (Fig. 6 inset) the sensitivity of composite-3 modified GCE is 16 μA μM^{-1} cm^{-2}, and the correlation coefficient is 0.9357. From the same results, limit of detection (LOD) of H_2O_2 at composite-3 film with a signal to noise ratio of 3 is 30 nM. The overall view of this result reveals that composite-3 film is efficient for H_2O_2 analysis. To study the reproducibility of the electrode fabrication, four individual electrodes were fabricated and their cyclic voltammograms recorded. The current was measured for the oxidation of 0.2 μM H_2O_2 in N_2 saturated PBS. The electrodes showed a relative standard deviation (RSD) of 6.96%.

3.5. DPV and selectivity studies of H_2O_2 at graphene–HRP multimer film

Fig. 7 shows the differential pulse voltammograms recorded for the addition of different H_2O_2 concentrations at composite-3 modified GCE in PBS. After each successive H_2O_2 addition, pre-purified N_2 gas was purged into PBS for 1 min before recording the next differential pulse voltammogram. From the corresponding differential pulse voltammograms, the I_{pc} values were plotted against H_2O_2 concentrations as shown in Fig. 7 inset. From this inset plot, it is obvious that composite-3 film exhibits a steady state response towards the addition of various H_2O_2 concentrations, and the reduction peak current increases linearly from 10 nM to 0.22 μM H_2O_2. From the slopes of linear calibration curve the sensitivity of composite-3 film modified GCE is 7.8 μA μM^{-1} cm^{-2}, and the correlation coefficient is 0.9947. Similarly, LOD of H_2O_2 at composite-3 film with a signal to noise ratio of 3 is 9 nM. In general, DPV results reveal that graphene–HRP multimer film is efficient for H_2O_2 determination. The comparison of composite-3 modified GCE with previously reported electrodes (Table 1) reveals composite-3 exhibits lower overpotential for H_2O_2 reduction and lower detection limit for H_2O_2 determination. The DPV experiments for selectivity studies were carried out using various analytes such as ascorbic acid, acetic acid, uric acid and dopamine. In selectivity experiments the concentration of H_2O_2 was kept constant at 0.22 μM, and then 0.2 mM of each analyte was added. The results show that the I_{pc} values of H_2O_2 before and after addition of the analytes do not vary obviously (ESI‡). The stable I_{pc} value is due to the fact that the overpotential window of the interfering compounds is not same as that of H_2O_2 reduction potential at composite-3. These DPV results indicate that composite-3 film can be used for H_2O_2 determination in real samples.

3.6. Real sample analysis of H_2O_2 using graphene–HRP multimer film

The performance of composite-3 modified GCE in real sample analysis was tested by applying it to the determination of H_2O_2 in

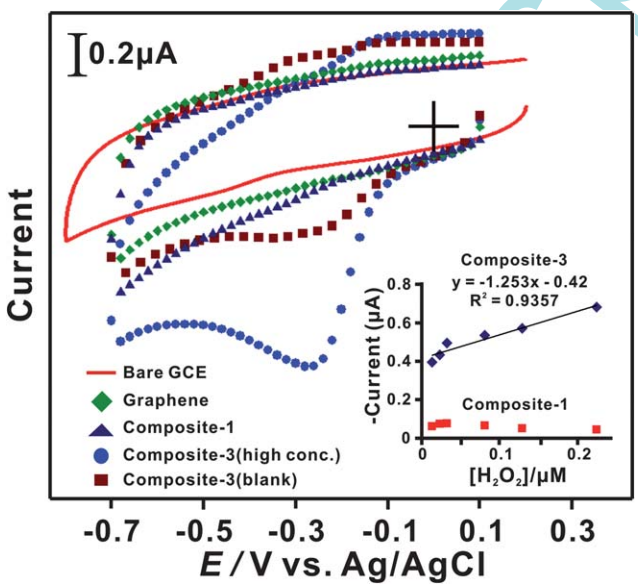

Fig. 6 Cyclic voltammograms of H_2O_2 (0.22 μM) at bare GCE, graphene, composite-1 and composite-3 modified GCEs in PBS at 50 mV s^{-1}; where composite-3 is shown both in the absence and presence of 0.22 μM H_2O_2. The inset is the plot of peak current *vs.* concentration of H_2O_2 for composite-1 and composite-3.

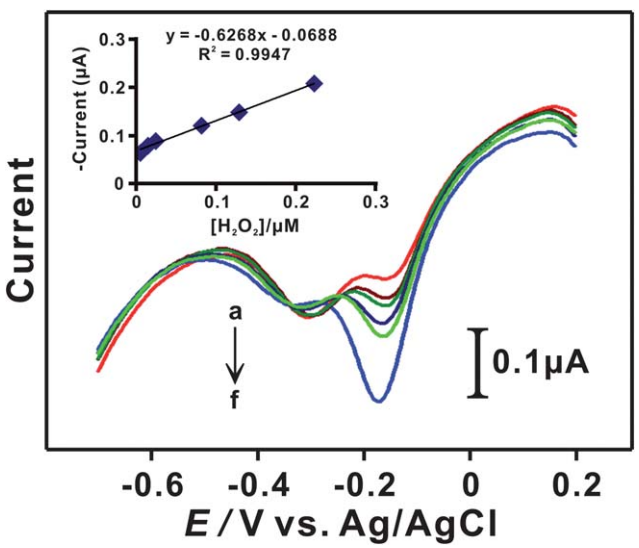

Fig. 7 Differential pulse voltammograms of H_2O_2 (*a–f* = 4.98 nM to 0.22 μM) at composite-3 modified GCE in PBS. Inset represents the plot of peak current (I_{pc}) *vs.* concentration of H_2O_2 at composite-3 modified GCE.

Table 1 Comparison of electroanalytical results of H_2O_2 at various modified electrodes in various conditions

Electrodes	pH	E_{pa}/E_{pc} (V)	Linear range	Sensitivity	LOD	Ref.
Composite-3	7.0	−0.16	10 nM to 0.22 μM	7.8 μA μM^{-1} cm^{-2}	9 nM	This work
HRP/laponite/chitosan	7.0	−0.13	29 μM to 1.4 mM	19.7 mA M^{-1} cm^{-2}	5 μM	29
Graphene oxide sheet-prussian blue	5.0	0.2	0.05 to 140 mM	—	—	30
Graphene oxide/prussian blue	6.0	0.1	5.0 μM to 1.2 mM	408.7 μA mM^{-1} cm^{-2}	0.12 μM	31
MB/MWCNT/CF[a]	7.2	−0.33	1 μM to 0.7 mM	—	1 μM	32
Spinach ferredoxin	7.0	−0.2	—	68.24 μA mM^{-1} cm^{-2}	—	33
Ni/Al-LDHs[b]	13.0	0.06	0.036 to 175 μM	74.82 μA mM^{-1}	9 nM	34
Co/Al-LDHs[b]	13.0	0.49	0.2 to 674 μM	97.61 μA mM^{-1}	50 nM	34
Roughened macroporous Au-/nPts[c]	7.4	0.1	—	264 μA mM^{-1} cm^{-2}	50 μM	35
PP-GCE[d]	7.0	−0.35	1 to 80 μM	0.000967 μA μM^{-1}	1 μM	36
$(NGB/LDH)_6$[e]	13.0	0.38	8 μM to 0.18 mM	—	0.9 μM	37
Diazo-ATP monolayer[f]	6.0	−0.25	1.0 μM to 6.38 mM	—	0.67 μM	38

[a] MB – methylene blue; MWNT – multiwall carbon nanotube; CF – ciprofloxacin. [b] LDHs – layered double hydroxides. [c] nPts – nanoparticles. [d] PP – *p*-nitrophenyl phosphate. [e] NGB – naphthol green B. [f] ATP – 4-aminothiophenol.

Table 2 Electroanalytical values obtained for H_2O_2 determination in real sample using DPV in PBS at composite-3 film modified GCE

Added (nM)	Found (nM)	Recovery (%)	RSD (%)
14.8	13.9	92	1.5
24.4	19.5	94	
33.8	28.7	96	

commercially available H_2O_2 solution. DPV was used with same experimental conditions described in section 3.5. The H_2O_2 solution was obtained from Jen Sheng Pharmaceutical Co. Ltd., Taiwan. The concentrations added in the experiment, found and RSD obtained from the experiments are given in Table 2. From the results, the recovery of H_2O_2 was ≈94%, based on the assumption that the composition was exactly as mentioned by the manufacturer. These above results show that composite-3 film is efficient for H_2O_2 determination.

4. Conclusion

We demonstrated a simple method for fabrication of graphene–HRP multimer film on GCE. The developed graphene–HRP multimer film showed good electrocatalytic activity for the reduction of H_2O_2. Graphene–HRP multimer has the combined advantages of ease of fabrication, high reproducibility and sufficient stability. SEM and AFM results have shown the difference between the graphene and HRP multimer structures. Further, graphene–HRP multimer film has good functional properties together with electrocatalytic activity on H_2O_2. CV and DPV techniques used for graphene–HRP multimer film characterization in this article provide an opportunity for qualitative and quantitative characterization of this H_2O_2 sensor.

Acknowledgements

This work was supported by the National Science Council and the Ministry of Education of Taiwan (Republic of China).

References

1 A. K. Geim and K. S. Novoselov, *Nat. Mater.*, 2007, **6**, 183–191.
2 M. Pumera, A. Ambrosi, A. Bonanni, E. L. K. Chng and H. L. Poh, *TrAC, Trends Anal. Chem.*, 2010, **29**, 954–965.
3 S. Alwarappan, A. Erdem, C. Liu and C. Z. Li, *J. Phys. Chem. C*, 2009, **113**, 8853–8857.
4 A. Ambrosi and M. Pumera, *Chem.–Eur. J.*, 2010, **16**, 10946–10949.
5 T. T. Baby, S. S. J. Aravind, T. Arockiadoss, R. B. Rakhi and S. Ramaprabhu, *Sens. Actuators, B*, 2010, **145**, 71–77.
6 J. Li, S. Guo, Y. Zhai and E. Wang, *Electrochem. Commun.*, 2009, **11**, 1085–1088.
7 Y. Wang, Y. Li, L. Tang, J. Lu and J. Li, *Electrochem. Commun.*, 2009, **11**, 889–892.
8 Y. R. Kim, S. Bong, Y. J. Kang, Y. Yang, R. K. Mahajan and J. S. Kim, *Biosens. Bioelectron.*, 2010, **25**, 2366–2369.
9 R. Huang and N. Hu, *Bioelectrochemistry*, 2001, **54**, 75–81.
10 Z. J. Wang, M. Y. Li, P. P. Su, Y. J. Zhang and L. Niu, *Electrochem. Commun.*, 2008, **10**, 306–310.
11 P. A. MacCarthy and A. M. Shah, *Coron. Artery Dis.*, 2003, **14**, 109–113.
12 R. Rodrigo and G. Rivera, *Free Radical Biol. Med.*, 2002, **33**, 409–422.
13 W. Chen, S. Cai, Q. Q. Ren, W. Wen and Y. D. Zhao, *Analyst*, 2012, **137**, 49–58.
14 M. Goldberg, M. Grootveld and E. Lynch, *Clin. Oral Invest.*, 2010, **14**, 1–10.
15 E. Kim, K. Kim, H. Yang, Y. T. Kim and J. Kwak, *Anal. Chem.*, 2003, **75**, 5665–5672.
16 M. Delvauxa, A. Walcarius and S. Demoustier-Champagne, *Anal. Chim. Acta*, 2004, **525**, 221–230.
17 Z. Matharu, P. Pandey, M. K. Pandey, V. Gupta and B. D. Malhotra, *Electroanalysis*, 2009, **21**, 1587–1596.
18 M. J. B. Wissink, R. Beernink, J. S. Pieper, A. A. Poot, G. H. M. Engbers and T. Beugeling, *Biomaterials*, 2001, **22**, 151–163.
19 M. J. van Luyn, P. B. van Wachem, L. O. Damink, P. J. Dijkstra, J. Feijen and P. Nieuwenhuis, *J. Biomed. Mater. Res.*, 1992, **26**, 1091–1110.
20 P. B. van Wachem, M. J. van Luyn, L. H. O. Damink, P. J. Dijkstra, J. Feijen and P. Nieuwenhuis, *Int. J. Artif. Organs*, 1994, **17**, 230–239.
21 P. B. van Wachem, M. J. van Luyn, L. H. O. Damink, P. J. Dijkstra, J. Feijen and P. Nieuwenhuis, *J. Biomed. Mater. Res.*, 1994, **28**, 353–263.
22 *Soft Matter Gradient and Surfaces – Methods and Applications*, ed. J. Genzer, John Wiley & Sons, Inc., New Jersey, 2012, ISBN: 978-1-1181-6607-9.
23 G. M. Morris, D. S. Goodsell, R. S. Halliday, R. Huey, W. E. Hart and R. K. Belew, *J. Comput. Chem.*, 1998, **19**, 1639–1662.
24 J. Fuhrmann, A. Rurainski, H. P. Lenhof and D. Neumann, *J. Comput. Chem.*, 2010, **31**, 1911–1918.
25 H. O. Finklea, D. A. Snider and J. Fedyk, *Langmuir*, 1993, **9**, 3660–3667.
26 A. Das, B. Chakraborty and A. K. Sood, *Bull. Mater. Sci.*, 2008, **31**, 579–584.
27 R. S. Dey and C. R. Raj, *J. Phys. Chem. C*, 2010, **114**, 21427–21433.
28 C. C. Chen and Y. Gu, *Biosens. Bioelectron.*, 2008, **23**, 765–770.

29 D. Shan, Q. B. Li, S. N. Ding, J. Q. Xu, S. Cosnier and H. G. Xue, *Biosens. Bioelectron.*, 2010, **26**, 536–541.
30 X. W. Liu, Z. J. Yao, Y. F. Wang and X. W. Wei, *Colloids Surf., B*, 2010, **81**, 508–512.
31 Y. Zhang, X. Sun, L. Zhu, H. Shen and N. Jia, *Electrochim. Acta*, 2011, **56**, 1239–1245.
32 S. A. Kumar, S. F. Wang, Y. T. Chang, H. C. Lu and C. T. Yeh, *Colloids Surf., B*, 2011, **82**, 526–531.
33 A. K. Yagati, T. Lee, J. Min and J. W. Choi, *Bioelectrochemistry*, 2011, **80**, 169–174.
34 Z. Yin, J. Wu and Z. Yang, *Biosens. Bioelectron.*, 2011, **26**, 1970–1974.
35 Y. J. Lee, J. Y. Park, Y. Kim and J. W. Ko, *Curr. Appl. Phys.*, 2011, **11**, 211–216.
36 S. Han, Y. Yuan, L. Hu and G. Xu, *Electrochem. Commun.*, 2010, **12**, 1746–1748.
37 X. Kong, J. Zhao, J. Han, D. Zhang, M. Wei and X. Duan, *Electrochim. Acta*, 2011, **56**, 1123–1129.
38 F. Li, Y. Feng, L. Yang and S. Liu, *Talanta*, 2010, **83**, 205–209.

